Journal of
Materials Chemistry B

Materials for biology and medicine

Accepted Manuscript

This article can be cited before page numbers have been issued, to do this please use: I. Veronika Judith Feiner, K. R. Pulagam, K. B. Uribe, R. Passannante, C. Simó, K. Zamacola, V. Gómez-Vallejo, N. Herrero, U. Cossío, Z. Baz, M. M. Caffarel, C. H. Lawrie, D. J. Vugts, L. Rejc and J. Llop, *J. Mater. Chem. B*, 2020, DOI: 10.1039/D0TB01880E.

ROYAL SOCIETY OF CHEMISTRY

rsc.li/materials-b

View Article Online
DOI: 10.1039/D0TB01880E

ARTICLE

Pre-targeting with ultra-small nanoparticles: Boron carbon dots as drug candidates for boron neutron capture therapy

Received 00th January 20xx,
Accepted 00th January 20xx

DOI: 10.1039/x0xx00000x

Irene V. J. Feiner, [a] Krishna R. Pulagam,[a] Kepa B. Uribe,[a] Rossana Passannante,[a] Cristina Simó,[a] Kepa Zamacola,[a] Vanessa Gómez-Vallejo,[a] Natalia Herrero-Álvarez,[a] Unai Cossío,[a] Zuriñe Baz,[a] María M. Caffarel,[b,c] Charles H. Lawrie,[b,c,d] Danielle J. Vugts,[e] Luka Rejc [a,f] and Jordi Llop [a,g,*]

Boron neutron capture therapy (BNCT) is a promising cancer treatment exploiting the neutron capture capacity and subsequent fission reaction of boron-10. The emergence of nanotechnology has encouraged the development of nanocarriers capable to accumulate boron atoms preferentially in tumour cells. However, long circulation time, required for high tumour accumulation, is usually paired by accumulation of the nanosystem in organs such as the liver and the spleen, which may cause off-target side effects. This could be overcome by using small-sized boron carriers under a pretargeting strategy. Here, we report the preparation, characterisation and *in vivo* evaluation of tetrazine-functionalised boron-rich carbon dots, which show very fast clearance and low tumour uptake after intravenous administration in a mouse HER2 (human epidermal growth factor receptor 2)-positive tumour model. Enhanced tumour accumulation was achieved when using a pretargeting approach, which was accomplished by a highly selective biorthogonal reaction at the tumour site with trans-cyclooctene-functionalised Trastuzumab.

Introduction

In spite of recent advances, cancer remains one of the leading causes of death world-wide. New therapeutic approaches are urgently needed to improve patient outcome, increase treatment efficacy and reduce side effects.[1] Binary approaches for cancer therapy, based on the combination of two non- or low-toxic components that become effective only when co-localised, have been developed over the last years to overcome the limitations of traditional therapies. One of such approaches is boron neutron capture therapy (BNCT).[2] In BNCT, boron-10 (^{10}B) atoms selectively delivered to tumour cells are submitted to neutron irradiation, causing a nuclear reaction, which results in the emission of α particles and ^{7}Li recoil ions. These particles have high linear energy transfer, which induces DNA-double strands breaks, triggering cell death.[3, 4]

BNCT was first proposed more than 80 years ago.[2] However, and in spite of decades of efforts and development of potential BNCT agents,[5] one of the major limitations for the clinical application of BNCT is still the lack of drugs capable of delivering a sufficient amount of boron atoms to tumour cells. Indeed, only two boronated compounds are currently used in clinical trials: (L)-4-dihydroxy-borylphenylalanine, commonly known as boronophenylalanine (BPA); and sodium mercaptoundecahydro-*closo*-dodecaborate, commonly known as sodium borocaptate (BSH).[6, 7] Still, they show low tumour selectivity and are only effective against certain types of cancer.

The lack of success in the development of promising drug candidates and the inconvenience of conducting clinical trials in the vicinity of nuclear reactors temporarily discouraged the development of BNCT and its clinical application. However, two recent advances have shifted the paradigm of this therapeutic modality: first, the development of accelerators capable to generate high intensity neutron beams,[8-10] which enable treating patients in a user-friendly environment and at a lower cost; second, the emergence of nanotechnology, which has triggered the development of nanoparticle (NP)-based boron carriers, capable to passively accumulate in tumour tissues taking advantage of the enhanced permeability and retention (EPR) effect. To date, different nanosized platforms have been proposed as boron carriers[11, 12] including liposomes,[13-15] iron oxide nanoparticles,[16-18] carbon[19, 20] and boron nitride[21, 22] nanotubes, and gold nanoparticles,[23-25] among others. However, NPs usually exhibit long circulation times and uptake in organs of the mononuclear phagocytic system (MPS) such as the liver and the spleen, which may result in eventual toxic, off-target side effects and limit

[a] CIC biomaGUNE, Basque Research and Technology Alliance (BRTA), San Sebastian, Spain.
[b] Biodonostia Health Research Institute, San Sebastian, Spain.
[c] IKERBASQUE, Basque Foundation for Science, Bilbao, Spain.
[d] Radcliffe Department of Medicine, University of Oxford, Oxford, UK.
[e] Amsterdam UMC, Vrije Universiteit Amsterdam, Dept. Radiology & Nuclear Medicine, The Netherlands
[f] University of Ljubljana, Faculty of Chemistry and Chemical Technology, Večna pot 113, 1000 Ljubljana, Slovenia.
[g] Centro de Investigación Biomédica en Red, Enfermedades Respiratorias - CIBERES.
† Footnotes relating to the title and/or authors should appear here.
Electronic Supplementary Information (ESI) available: Detailed experimental methods, additional characterisation data. See DOI: 10.1039/x0xx00000x

repeated administration. To circumvent this, we envisaged the application of a pre-targeting approach, as previously described in the fields of imaging and targeted-radionuclide therapy.[26] In a typical pre-targeting experiment, a monoclonal antibody (mAb), functionalised with *trans*-cyclooctene (TCO), is injected into the subject. After blood clearance (24–72 hours), a radiolabelled small molecule, functionalised with a tetrazine (tz) moiety and capable of undergoing a fast bioorthogonal reaction with TCO (inverse-electron-demand Diels-Alder cycloaddition), is injected. The small labelled molecule distributes through all tissues but only reacts with the mAb-TCO, which is present in e.g. the tumour.[27-30]

In our quest to develop nanomaterial-based BNCT agents, and inspired by previous works in the context of atherosclerosis,[31] we hypothesized that tz moieties, attached to the surface of small boron-rich NPs, could undergo the click-reaction with TCO-mAb. This would give a base for the pre-targeting approach that would lead to the desired selectivity of boron-rich NPs and provide with a valuable alternative to current nanomaterial-based BNCT agents (Fig. 1).

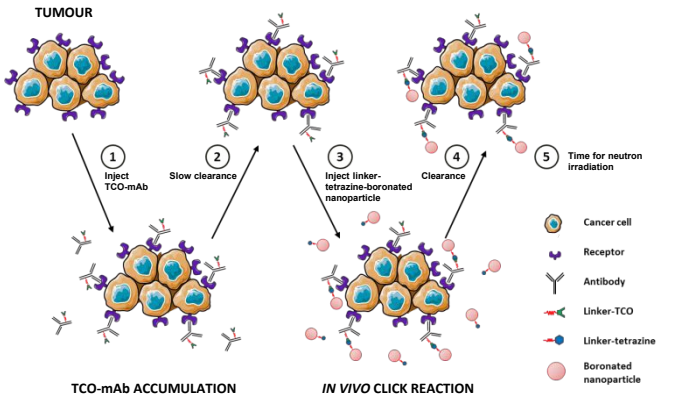

Figure 1. Schematic representation of the pre-targeting strategy using small boron-rich nanoparticles: The TCO-functionalised antibody is administered and accumulates in the tumour (1). After clearance (2), boron-rich, tetrazine functionalised NPs (3) are injected. Those reaching the tumour undergo bioorthogonal reaction and are selectively retained, while non-reacted particles are cleared (4). At the final stage, neutron irradiation can be applied (5).

Here, we report the preparation and characterization of boron-doped carbon dots (B-CDs), functionalized with a tz moiety to enable pre-targeting. For our proof of concept experiments, we selected a xenograft mouse model of breast cancer, generated by subcutaneous inoculation of BT-474 cells, which over-express human epidermal growth factor (HER2) receptors, in immunodefficient mice. As targeting counterpart, TCO-functionalized Trastuzumab, a well-known, FDA-approved humanized mAb with high target specificity and binding affinity to HER2 receptors, was used. Radiolabelling of both, the mAb and the nanosystem, followed by positron emission tomography (PET) in combination with computed tomography (CT) imaging was used to: (i) determine the optimal time for administration of the boron carrier; and (ii) indirectly quantify the amount of boron accumulated in the tumour.

Experimental

View Article Online
DOI: 10.1039/D0TB01880E

Materials and methods

Reagents: All reagents were obtained from Sigma-Aldrich (analytical grade purity) unless otherwise stated. Milli-Q water (resistivity 18.2 MΩ·cm at 25 °C) was obtained from a Milli-Q A10 Gradient equipment (Millipore). NHS-Cy3 was purchased from BroadPharm. *p*-NCS-Bz-DFO was obtained from CheMatech and mTzCy3 from Jena Bioscience. The antibody Trastuzumab was purchased from Roche Pharma, S.A. (Spain). [^{89}Zr]ZrC_2O_4 (in 1 M oxalic acid) was produced in house with an IBA Cyclone 18/9 cyclotron using a (p, n) reaction on natural yttrium-89, and isolated with a hydroxamate column following standard protocol.[32] [^{131}I]NaI (in 0.1 M NaOH) was purchased from PerkinElmer. BT-474 cells were purchased from ATCC. Animals were purchased from Charles River Laboratories (France).

Instrumentation: Successful preparation of synthetic products was confirmed by NMR spectroscopy. NMR spectra of $CDCl_3$ or acetonitrile-d_3 solutions were recorded on a Bruker Avance III 500 MHz spectrometer at 302 K. The chemical shifts (δ) are reported in *parts per million* (*ppm*) and are referenced to the deuterated solvent used. The coupling constants (*J*) are reported in Hz, and the splitting patterns are indicated as s (singlet), d (doublet), dd (doublet of doublets), t (triplet), and tt (triplet of triplets).

The synthesis of B-CDs was performed using a CEM Focused Microwave™ Synthesis System, Discover® SP. The FTIR spectra were recorded on a Fourier-transform infrared spectrometer (ThermoScientific Nicolet 6700), using dry B-CDs powder as the sample with potassium bromide (KBr) as the matrix. Atomic force microscopy (AFM) studies were performed using a Veeco Multimode AFM attached to a Nanoscope V controller. The sample was imaged in tapping mode in air, using TESPA-V2 doped silicon probe with k = 42 N/m. A drop of a diluted solution of the particles was placed on a glass substrate, the sample left to evaporate at room temperature and afterwards imaged.

UV-Vis spectra were measured in an Agilent 8453 UV-Vis-NIR diode-array spectrophotometer. ζ-potential was measured in 10 mM phosphate buffered saline solution (PBS; pH = 7.4) using a Malvern Zetasizer Nano ZS system (Malvern Instruments, Malvern, UK). X-ray Photoelectron Spectroscopy (XPS) experiments were performed in a SPECS Sage HR 100 spectrometer (Berlin, Germany) with a non-monochromatic X ray source (aluminium Kα line of 1486.6 eV energy and 252 W), placed perpendicular to the analyser axis and calibrated using the 3d5/2 line of Ag with a full width at half maximum (FWHM) of 1.1 eV. The selected resolution for the spectra was 15 eV of Pass Energy and 0.15 eV/step. All measurements were made in an ultra-high vacuum (UHV) chamber at a pressure around 6 × 10^{-8} mbar. An electron flood gun was used for charge neutralization. Gaussian Lorentzian functions were used for fittings (after a Shirley background correction) where the FWHM of all the peaks were constrained while the peak positions and areas were set free. Main C1s peak was used for charge reference and set at 284.8 eV.

View Article Online
DOI: 10.1039/D0TB01880E

ICP-MS measurements were performed on a Thermo iCAP Q ICP-MS (Thermo Fisher Scientific GmbH, Bremen, Germany), coupled to an ASX-560 autosampler (CETAC Tech, Omaha, NE, USA). For sample preparation, the B-CDs or B-CDs-Tz (determination of boron content in the dots) or the cells (determination of B-CD-Tz internalisation) were immersed in aqueous HNO_3 solution (70%, 1:1 with sample). The dispersion was left overnight until the solution became clear. The solution was then diluted with 2% HNO_3 to 10 mL and analysed.

HPLC analysis was carried out using an Agilent 1200 series HPLC equipped with a quaternary pump, a multiple wavelength detector and a radiometric detector (Gabi, Raytest).

Fluorescence spectra were measured at room temperature using a Perkin Elmer (LS 55) fluorimeter. Excitation source: Pulsed Xenon lamp 8 W; detector: PMT (200–650 nm); polarizers anisotropy/polarisation measurements; emission monochromator cut off filter set: 290, 350, 390, 430 and 515 nm, attenuator 1 % T; FL-WinLab software for data acquisition and analysis. Cell observer microscopy experiments were carried out using a Zeiss Axio Observer Fluorescence microscope using Ibidi clear bottomed µ-slide 8-well microscopy plates and analysed by ZEN2012-ZEISS.

Gamma counts were measured using a Wallach Wizard, PerkinElmer (Waltham, MA, USA) gamma counter. Radio-thin layer chromatography (radio-TLC) was performed using silica gel coated aluminium sheets and methanol/dichloromethane 3:7 as the stationary and mobile phases, respectively. TLC plates were analysed using a TLC-reader (MiniGITA, Raytest).

PET experiments were performed using an eXploreVista-CT small animal PET-CT system (GE Healthcare). Anaesthesia was induced with 3–5 % isoflurane and maintained by 1.5–2.0 % of isoflurane in 100 % O_2.

Chemistry and Radiochemistry

Conjugation of TCO-NHS to Trastuzumab: The mAb Trastuzumab (21 mg/mL, 2 mg) was diluted with PBS to a concentration of 3.0 mg/mL. The pH was adjusted to 8.6–9.1 with 0.1 M Na_2CO_3. *Trans*-Cyclooctene (TCO-NHS, 20 mM in DMSO, 50–55 eq.) was added. After incubation (120 min, room temperature) non-reacted TCO-NHS was removed by spin filtration (100 kDa, 12000 rpm) and the conjugated mAb washed three times with PBS. After recovering the mAb from the filter with PBS its concentration was determined by NanoDrop®, using the default extinction coefficient for immunoglobulin type mAbs: ε(mAb) = 210 L/(mmol x cm).

To determine the TCO/mAb ratio, an aliquot of the TCO-conjugated mAb (0.05 mg) was taken and 5–10 molar eq. 6-methyl-tetrazine-sulfo-Cy3 (mTzCy3, 1 mg/mL in DMSO) were added. After 5 min incubation at room temperature, the fluorophore-labelled mAb was purified by spin filtration (100 kDa, 12000 rpm) and washed four times with PBS. After recovering the mAb from the filter with PBS, the concentrations of mAb and mTzCy3 were determined by NanoDrop®. The following extinction coefficients were used: ε(mAb) = 210 L/(mmol x cm), NanoDrop® default for immunoglobulin type mAbs; and ε(mTzCy3) = 151 L/(mmol x cm), taken from datasheet of Jena Bioscience. Finally, the ratio between mTzCy3 and mAb was calculated.

Conjugation of *p*-NCS-Bz-DFO to Trastuzumab: The mAb Trastuzumab (21 mg/mL, 2 mg) was diluted with PBS to a concentration of 3.0 mg/mL. The pH was adjusted to 8.6–9.1 with 0.1 M Na_2CO_3. *p*-NCS-Bz-DFO (5 mM in DMSO, 5 eq.) was added. After incubation for 45 min at 37 °C, purification was performed by spin filtration (100 kDa, 12000 rpm) and the conjugated mAb washed three times with PBS. The mAb was recovered from the filter with PBS and its concentration was determined by NanoDrop®.

Synthesis of B-CDs and functionalization with tetrazine: To a 10 mL microwave vessel were added citric acid monohydrate (1 eq., 18.0 mg), ethylendiamine (10 eq., 57.0 µL), sodium tetraborate (3 eq., 51.7 mg) and 300 µL MilliQ water. The vial was capped and placed in the microwave. The reaction was carried out at 220 °C, 200 W, 370 PSI, stirring for 5 min with 2 min ramp time. Purification was performed by sephadex size exclusion column (NAP5® GE Healthcare) using water as the eluent, and the collected fractions were lyophilized. The obtained particles were analysed by AFM, XPS, FT-IR, ICP-MS and for their fluorescence.

To attach tetrazine (tz), B-CDs (6 mg) were dissolved in PBS (500 µL). The solution had a pH ≈ 9 and tz-PEG_5-NHS (1.6 mg in 30 µL DMSO, 110 mM) was added without further adjustment of the pH. After incubation overnight, purification was performed by sephadex size exclusion column (NAP5® GE Healthcare) using water as the eluent, and the collected fractions lyophilized. The obtained particles were analysed by ICP-MS, HPLC, for their fluorescence, internalization and cytotoxicity.

Radiolabelling of Trastuzumab with ^{89}Zr: Radiolabelling of the DFO-Trastuzumab with ^{89}Zr was performed by incubation with [^{89}Zr]ZrC_2O_4 in a 1 M oxalic acid solution. For this, oxalic acid (1 M; 50 µl) containing ^{89}Zr (ca. 20 MBq) was neutralized with 2 M sodium carbonate (ca. 23 µL). The mAb (450 µg) was then added and the volume was adjusted to 0.5 mL with 0.5 M HEPES buffer. After 1 h incubation at room temperature the mAb was purified by sephadex G-25 size exclusion column (NAP5® GE Healthcare) and PBS as the eluent. The incubation and purification was monitored by iTLC (mobile phase: 20 mM citric acid + 60 mM EDTA 9:1 acetonitrile). Lindmo assay was performed to assure reactivity of the mAb was not impaired.

Radiolabelling of Trastuzumab with ^{131}I: An Eppendorf tube was coated with 75 µg Iodogen (1,3,4,6-tetrachloro-3α,6α-diphenyl glycoluril). Sodium phosphate buffer (0.5 M; 50 µL), sodium phosphate buffer (0.1 M; 427 µL) and Trastuzumab (21 mg/mL; 19 µL) were added, followed by [^{131}I]NaI (4 µL; ca. 7.4 MBq in 0.1 M NaOH). After 4 min incubation at room temperature, the reaction was quenched with ascorbic acid solution (25 mg/mL Milli-Q water, pH = 5; 100 µL). Labelling was monitored by iTLC (mobile phase: 20 mM citric acid + 60 mM EDTA). The radiolabelled mAb was purified using sephadex G-25 size exclusion column (PD10® GE Healthcare) and ascorbic acid solution (5 mg/mL in saline, pH ≈ 5) as the eluent. Radiochemical yield of the purified [^{131}I]I-Trastuzumab was 73 % and radiochemical purity was 99 %. Lindmo assay

View Article Online
DOI: 10.1039/D0TB01880E

was performed to assure reactivity of the mAb was not impaired.

Radiosynthesis of [^{18}F]FPyTFP: The precursor for the preparation of [^{18}F]FPyTFP was synthesized in a 3-step sequence as described previously[33] (see Scheme S1 and ESI for detailed synthetic process and characterisation data). The synthesis of [^{18}F]FPyTFP was performed using a TRACERlab FX_{FN} synthesis module (GE Healthcare) by ^{18}F-fluorination of the trifluoromethanesulfonate precursor, inspired by a previously described procedure.[33] In brief, Fluorine-18 (^{18}F) was generated in an IBA Cyclone 18/9 cyclotron by irradiation (target current = 44 µA) of ^{18}O-enriched water with high energy (18 MeV) protons via ^{18}O(p, n)^{18}F reaction. [^{18}F]F^- was trapped on a pre-conditioned Sep-Pak® Accell Plus QMA Light cartridge (Waters, Milford, MA, USA), and then eluted with a solution of Kryptofix $K_{2.2.2}$ (15 mg)/K_2CO_3 (3.5 mg) in a mixture of water (500 µL) and acetonitrile (1 mL). After complete elimination of the solvent by azeotropic evaporation, a solution containing the precursor (10 mg) in a mixture of *t*-butanol and acetonitrile (4/1, v/v; 0.5 mL) was added and the mixture was kept at 40 °C for 15 min. The crude reaction mixture was diluted with acetonitrile/water (1/1, v/v; 2 mL) and purified by HPLC using a RP Mediterranea Sea18 column (10 × 250 mm, 5 µm particle size; Teknokroma, Spain) as the stationary phase and acetonitrile/0.1% TFA in Milli-Q water (80/20, v/v) as the mobile phase at a flow rate of 3 mL/min. The desired fraction (t_R = 29–30 min) was collected, diluted with water (25 mL), and the radiotracer was retained on a C-18 cartridge (Sep-Pak® Light, Waters, Milford, MA, USA). The cartridge was washed with water (5 mL) and the radiotracer eluted with acetonitrile (1 mL). For the purpose of further use of the radiolabelled prosthetic group, [^{18}F]FPyTFP was used dissolved in acetonitrile as obtained after elution from the cartridge. Chemical and radiochemical purity were determined by HPLC using a Mediterranean C18 column (4.6 × 150 mm, 5 µm) as stationary phase and 0.1% TFA/acetonitrile (0–1 min 25% acetonitrile; 9–12 min 90% acetonitrile; 13–15 min 25% acetonitrile) as the mobile phase at a flow rate of 1.5 mL/min (retention time = 8.1 min).

Radiolabelling of B-CDs-tz with [^{18}F]FPyTFP: B-CDs-tz (1.2 mg) were dissolved in PBS (pH 7.4; 500 µL) and [^{18}F]FPyTFP in acetonitrile (296 MBq, 20 µL) was added. After 10 min incubation at 70 °C the labelling was complete as monitored by radio-TLC (silica gel 60 F254 on aluminium sheets (Merck), methanol/dichloromethane 3:7).

***In vitro* studies**

Cells: BT-474 cells were cultured in DMEM medium (Gibco), supplemented with 10 % fetal bovine serum and 1 % penicillin-streptomycin, at 37 °C with 5 % CO_2 in a humid atmosphere. Cells were confirmed to be free of mycoplasma contamination.

Lindmo assay: The assay was performed using the protocol of Lindmo,[34] using one concentration of mAb (10–15 ng/mL) and different dilutions of 0.5 mL BT-474 cells in PBS/1% BSA (2.8–0.2 × 10^6 cells/mL) in triplicates. The lowest concentration was prepared twice, the second set serving as non-specific binding (NSB) control (containing 2 µL of 5 mg/mL non-labelled mAb). To each cell dilution, 0.5 mL of radiolabelled Trastuzumab was added and incubated in a head over head rotator at 4 °C overnight. The cell suspensions were centrifuged, the supernatant (500 µL) separated and the amount of radioactivity in all samples (pellets and supernatants) measured in a gamma-counter. The amount of radioactivity measured from the supernatants was subtracted from the pellet activity to calculate the immunoreactive fraction.

Cytotoxicity studies: To determine cell viability, BT-474 human breast cancer cells were incubated with functionalized B-CDs over 48 h and 72 h. Cells were seeded (3 × 10^4 cells/well, 100 µL/well, 96-well plate), allowed to adhere overnight in complete media and maintained in a humid atmosphere at 37 °C and 5 % CO_2. Then, media was removed and cells were left untreated (control) or incubated with the B-CDs-containing formulations, diluted accordingly in media. The experiments were performed in triplicates. After the desired time, cell supernatant was removed and MTT reagent (100 µL/well; Roche), diluted in the corresponding media to the final concentration of 0.25 mg/mL, was added. After 1 h incubation at 37 °C and 5 % CO_2, the excess reagent was removed and formazan crystals were solubilized by adding DMSO (200 µL/well). The optical density of each well was measured in a TECAN Genios Pro 96/384 microplate reader at 550 nm. Data was represented as the percentage of cell survival (mean ± standard deviation, n = 3) compared to control wells.

***In vitro* internalization studies of B-CDs-tz-Cy3:** B-CDs-tz (2 mg/mL in PBS, 450 µL) were incubated with 25 µL TCO-Cy3 (10 mM in DMSO) for 5 min at room temperature. The particles were purified by sephadex size exclusion column (NAP5® GE Healthcare). The labelling was confirmed by UV-VIS spectra. BT-474 cells were seeded in a poly-L-Lysine treated 'Ibidi' µ-slide 8-well-plate (30,000 cells/well in 0.3 mL) and incubated overnight to adhere (37 °C, 5 % CO_2, humid atmosphere). The media was removed and 0.1 mL Hoechst 33342 (1 µg/mL medium) added to stain the nucleus. After 10 min incubation (37 °C, 5 % CO_2, humid atmosphere) 0.1 mL LysoTracker deep red (1 µg/mL in media) was added to stain the lysosomes. After 20 min incubation (37 °C, 5 % CO_2, humid atmosphere) media was removed and 0.3 mL of Cy3-labeled B-CDs (75 µg/mL medium) added. After 2 h incubation (37 °C, 5 % CO_2, humid atmosphere) the media was removed and replaced with fresh media. The images were taken with a Cell Axio Observer Fluorescence Microscope. Controls of single staining for each fluorophore were included. Images were analysed by ZEN-ZEISS software.

To determine the amount of boron that was actually internalised in the cells, parallel experiments were carried out under similar conditions (2h, 37 °C, OptiMEM), using 150,000 cells/well and a concentration B-CDs-tz of 250 µg/mL (62,5 µL from 1 mg/mL stock, in 250 µL final volume). After incubation and separation of the supernatant, the cells were processed and submitted to ICP-MS analysis. Cells incubated with only the media were also analysed as controls. To corroborate the results, internalization experiments were carried out with [^{18}F]B-CDs-Tz. BT474 cells (150,000 cells/well) were incubated with [^{18}F]B-CDs-Tz (75 µg/mL, 250 µL final volume) for 1 hour.

View Article Online
DOI: 10.1039/D0TB02180F

Cells were then washed twice with cold PBS, lysed with 1M NaOH and all fractions (media + washes + cells) analysed in the gamma counter. Internalization was calculated as the percentage cpm in the cell debris compared to cpm in media plus washes.

***In vivo* studies**

Animals: All animal experiments were performed in accordance with the Spanish policy for animal protection (RD53/2013), which meets the requirements of the European Union directive 2010/63/UE regarding the protection of animals used in experimental procedures. All experimental procedures were approved by the Ethical Committee of CIC biomaGUNE and authorized by the local authorities. All animals were housed in ventilated cages and fed on a standard diet *ad libitum*. The studies were performed on female NOD.CB17-Prkdcscid/J mice (Charles River).

Tumour growth: To grow BT-474 cell line breast cancer xenografts on female NOD.CB17-Prkdcscid/J mice, 5–6 weeks old mice were operated to implant a 17β-estradiol pellet (Belma Technologies) subcutaneously at their neck. The next day, 10×10^6 BT-474 tumour cells per animal were inoculated subcutaneously at the flank of the mouse. Prior to each inoculation, cells were diluted in sterile PBS:Matrigel (1:1). The sizes of the tumours were measured every 2–3 days with a digital calliper and volumes calculated (V= short diameter^2 x long diameter /2). At the time the tumour reached 200–300 mm^3 (around 2 weeks after inoculation) *in vivo* studies were performed.

***Ex vivo* studies to determine mAb internalization:** Trastuzumab was labelled in two batches, one with ^{89}Zr, the other one with ^{131}I. A mixture out of the two was created to obtain a 1:1 ratio of their activity (e.g. 0.185 MBq each). Four mice were injected intravenously, each with about 100 µg Trastuzumab in 100 µL PBS. *Ex vivo* studies were performed 24 h (n = 2) and 48 h (n = 2) post injection. Extracted organs were measured in a gamma counter (Wallach Wizard, PerkinElmer, Waltham, MA, USA) using a dual method enabling separate determination of ^{89}Zr and ^{131}I counts. The percentage of injected dose per gram (% ID/g) was calculated for the tumour uptake for each radionuclide.

***In vivo* PET imaging studies**: Female, BT-474 breast cancer xenograft-bearing mice were used. To determine the biodistribution of the mAb, [^{89}Zr]Zr-DFO-Trastuzumab (100 µg, 100 µL, 2.4-2.6 MBq) was injected via tail vein (n=3). Imaging studies were conducted using positron emission tomography (PET) in combination with computed tomography (CT) imaging, using an eXplore Vista-CT small animal PET-CT system (GE Healthcare). Static whole-body images (2 beds) were acquired at 1, 8, 24, 48 and 72 h after administration. PET images were analysed using PMOD image analysis software (PMOD Technologies Ltd, Zürich, Switzerland).

For proof of concept studies (evaluation of pre-targeting strategy), two groups of animals (n=3 per group) were used. The study group was injected with TCO-functionalized Trastuzumab (~2 TCO/mAb; approximately 100 µg in 100 µL) via tail vein. 24 h post injection the [^{18}F]B-CDs-tz (150–250 µg B-CDs-tz in 100 µL PBS, 7.4–11.1 MBq) were injected intravenously. The control group was only injected with [^{18}F]B-CDs-tz. Imaging studies were conducted using PET in combination with CT, using eXploreVista-CT small animal PET-CT system (GE Healthcare). Dynamic whole-body imaging (2 beds) was performed immediately after injection of [^{18}F]B-CDs-tz for 45 min. PET images were analysed using PMOD image analysis software (PMOD Technologies Ltd, Zürich, Switzerland). Values were expressed as percentage of injected dose per cubic centimetre (%ID/cm^3) (mean ± standard deviation; n = 3). Statistical analysis between groups at each time point was carried out using *t*-student test (two-tailed). Statistical significance was considered when $P < 0.05$.

Results and discussion

Synthesis and characterisation of boron carbon dots (B-CDs)

Among all the possibilities, we selected carbon dots (CDs), first described in 2004,[35] as the basic nanoplatform. The main selection criteria were the possibility to dope them with boron, their high biocompatibility and low toxicity and finally the rather fast and inexpensive synthesis.[36] Additionally, their small size (below 10 nm) promised fast elimination from circulation and tissues.[37]

Our first goal was to synthesise small-sized boron-rich carbon dots (B-CDs) bearing amine groups on the surface to enable subsequent functionalization. For this purpose, a microwave (MW) vial loaded with an aqueous suspension of citric acid, ethylenediamine, and sodium tetraborate, was submitted to 5 min MW heating (220 °C, 200 W, 370 PSI) (Fig. 2a). For all experiments described in this work, non-enriched sodium tetraborate was used to minimise costs (*ca.* 20% abundance of ^{10}B). The use of ^{10}B-enriched boron sources would be required to tackle BNCT experiments.

Purification using size exclusion (NAP5® G25 column) followed by lyophilisation yielded a beige fluorescent solid (Fig. 2b). Spherical particles, with a size distribution of 6.7 ± 1.8 nm (range: 3–10 nm, as determined by atomic force microscopy (AFM); Figure 2c) and with ζ-potential of -11.6 ± 0.8, were obtained. Consistent with AFM, size exclusion-high performance liquid chromatography (SE-HPLC) analysis of B-CDs showed the presence of several peaks, the main ones with retention time (t_R) in the range 4.8–7.0 min (Fig. S1a). XPS analysis (see ESI, Figure S2 for survey spectrum) confirmed the presence of oxygen, nitrogen, carbon and boron in the B-CDs. Five peaks were observed in the C-1s spectrum at 284.8, 286.0, 287.9, 288.8 and 282.8 eV, attributed to CC/CH, CO/CN, C=O, OC=C and CB bonds, respectively. Peaks at 192.1 eV (BCO_2/BO bonds) and 188.1 and 189.8 eV (BC and BN bonds, respectively) were also identified (Fig. 2d).[38] The percentage of boron in the B-CDs, as determined by ICP-MS, was 3.8 ± 0.4%. This value is similar to that reported previously for B-CDs synthesized using similar synthetic approaches.[39] The slight differences with respect to previously published results are most likely a due to different relative amounts of the three

components (citric acid, ethylenediamine, and sodium tetraborate) used in this synthetic procedure.

To gain further insight of the chemical structure, FTIR spectroscopy analysis was carried out to identify the functional groups present on B-CDs (Fig. 2e). The broad characteristic peak of O-H stretching was observed at 3420 cm^{-1}, together with a strong absorption band with maxima at 1610 and 1670 cm^{-1}, confirming the presence of carbonyl groups. In line with previously reported works, typical bands of citric acid were also present in the spectrum, including a broad peak at 3082 (attributed to the stretching of N–H groups), and 1350 cm^{-1} (attributed to C–N stretching). These bands suggest the presence of nitrogen atoms in the B-CDs. The presence of boron was also witnessed from FTIR spectrum, where bands at 1402 cm^{-1} (attributed to B–O stretching vibration), 1145 cm^{-1} (B–C absorption) and 1020 cm^{-1} (B-O-C) were observed. As expected, and in consonance with previous works,[39] no characteristic bands of aromatic compounds could be observed.

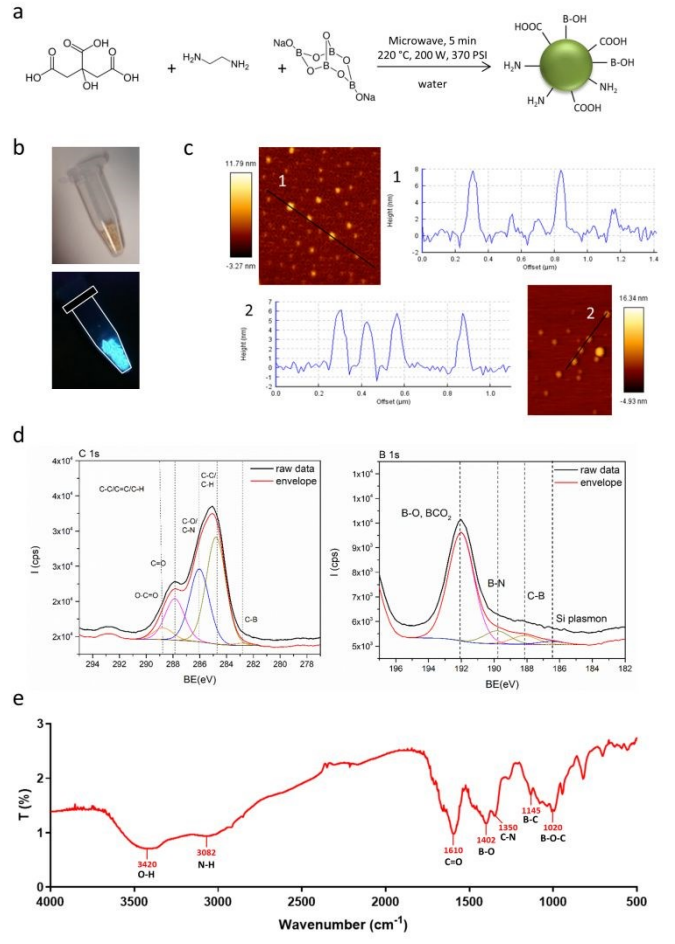

Figure 2. (a) Microwave-promoted reaction between citric acid, ethylenediamine, and sodium tetraborate to afford small-sized B-CDs in 5 min at 220 °C; (b) B-CDs after synthesis and lyophilisation (top), and under UV light (365 nm, bottom); (c) Representative AFM images to visualize shape and size of B-CDs. Lines on the images correspond to height profiles; (d) XPS high-resolution spectra of C-1s and B-1s of B-CDs; (e) FTIR spectrum of B-CDs.

The presence of free amino groups on the surface of the B-CDs enabled attachment of the tz moieties (Fig. 3a), which are required for the bioorthogonal reaction exploited in pre-targeting strategy. Successful attachment of tz was achieved via an S_N2 substitution reaction, using commercially available tz-PEG_5-NHS. A linker bearing five ethylene glycol units was used to increase the bio-compatibility of the resulting B-CDs.[40]

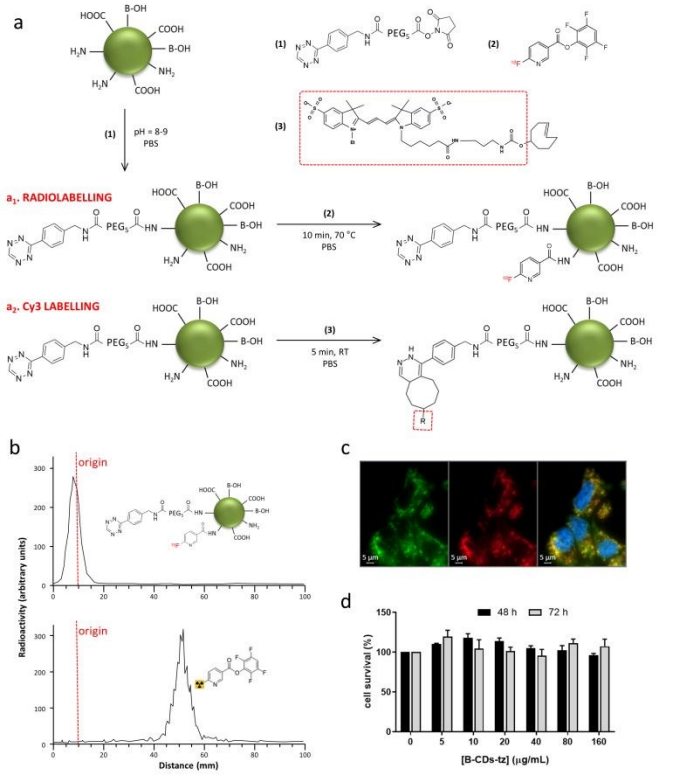

Figure 3. (a) Functionalisation of B-CDs with tz to yield B-CDs-tz; radiolabelling using [^{18}F]FPyTFP (a_1); and incorporation of the fluorophore Cy3 (a_2); (b) Radio-thin layer chromatograms monitoring the radiosynthesis of [^{18}F]FPyTFP-B-CDs-tz. Top: [^{18}F]B-CDs-tz after labelling was complete; bottom: [^{18}F]FPyTFP as control; (c) representative images by live cell fluorescence microscopy of functionalised B-CDs-tz after 2 h incubation. In green: B-CDs-tz, fluorophore-labelled with TCO-Cy3; in red: lysosomes, stained with Lysotracker-deep-red; in blue: nucleus, stained with Hoechst33342. Merged signals (B-CDs-tz co-localizing with lysosomes) appear in yellow; (d) cell viability in the presence of B-CDs-tz on BT-474 breast cancer cells; (mean ± standard deviation, n = 3).

Incubation of the B-CDs with tz-PEG_5-NHS at pH = 9 for 1 h and subsequent purification and lyophilisation yielded B-CDs-tz in an overall yield of ca. 15 %. After tz functionalization, ζ-potential values shifted from -11.6 ± 0.8 to -2.7 ± 0.3. Additionally, a shift of the main peak towards t_R = 10.1 min was observed with SE-HPLC (Fig. S1b). The longer t_R could be explained by non-exclusion effects, i.e. altered interactions with the stationary phase due to the presence of the tz moieties on the surface, rather than an actual modification of particle size.[41] The percentage of boron in the B-CDs-Tz, as determined by ICP-MS, was 3.4 ± 0.3%. Further confirmation of tz attachment was obtained by UV-Vis spectrophotometry, where the peak corresponding to the tz moiety (max absorbance at λ = 510 nm) could be clearly visualised (Figure

View Article Online
DOI: 10.1039/D0TB01880E

S3). Photoluminescence characterisation of B-CDs-tz showed maximum fluorescence intensities at similar excitation wavelengths as for B-CDs, 360 nm and 350 nm, respectively (Fig. S4). Contrary, functionalization severely affected emission intensity, which was 10-fold lower for B-CDs-tz at equivalent concentrations. Lyophilised samples were stable for at least 1 month when stored in the dark at room temperature, showing equivalent ζ-potential values and unaltered UV-Vis and fluorescence spectra.

Next, the click reaction between B-CDs-tz and TCO-functionalised Trastuzumab (on average 2 TCO groups per mAb molecule, see experimental section for details) was investigated *in vitro*. Mixtures with different TCO-mAb/B-CDs-tz ratios were incubated for 1 min and then analysed by SE-HPLC. Multiple peaks were observed in the chromatograms of the reaction mixtures (Figure S5). Apart from the set of peaks characteristic for free B-CDs-tz (major peak at t_R = 10.1 min), a new peak appeared at the same t_R as the mAb (t_R = 4.5 min). Progression of the click-reaction was determined by the decrease of the area under the peaks with t_R = 6–12 min (free B-CDs-tz) parallel to the increase of the area under the peak with t_R = 4.5 min (B-CDs-tz bound to mAb) (Figure S5). The experiments revealed that completion of the reaction was achieved in 5 min with a TCO-mAb to B-CDs-tz ratio ≥ 20:1.

Preliminary *in vitro* and *in vivo* studies

Internalization capacity and toxicity of B-CDs: Before moving to *in vivo* experiments, the internalisation capacity and cytotoxicity of the B-CDs-tz were evaluated in BT-474 cells, used to generate the tumour model (see below).

Direct evaluation of the internalisation was not possible due to low fluorescence signal intensity of B-CDs-tz (Figure S4). Hence, the CDs were decorated with fluorescent dye Cy3, through a click reaction between B-CDs-tz and Cy3-TCO (Fig. 3a). The cells themselves were stained for the nucleus and lysosomes with Hoechst33342 and Lysotracker-deep-red, respectively. Fluorescence microscopy images obtained after 2-hour incubation at 37 °C showed co-localization of the dots and the lysosomes, confirming internalisation of B-CDs-Cy3 conjugate (Fig. 3c). ICP-MS results confirmed that, under these experimental conditions, the amount of boron in the cells was 5 ng per well. Considering that each well contained 62.6 µg of B-CDs-Tz and that these contain ca. 3.4% boron, our results suggest that ca. 0.2% of the dots were actually internalised under our experimental conditions. These values were encouraging. As each well contained 150,000 cells, the amount of B per cell was calculated as 3.3 x 10^{-14} g/cell, which is equivalent to *ca.* 1.9 x 10^9boron atoms per cell. It is generally accepted that *ca.* 10^9 B atoms per cell suffice for an effective BNCT teratment.

It is worth mentioning that the values obtained by ICP-MS were quite close to the quantification limit of the technique, and a significant background was obtained when cells incubated in the absence of B-CDs-tz were analysed (control experiments). Because of this, internalisation experiments were also performed with [^{18}F]B-CDs-Tz, which was expected to be more sensitive and overcoming the limitation of the background signal. Internalization values of 0.12 ± 0.02% were obtained, thus confirming that both approaches provide similar results. The lower values obtained in assays using radiolabelled B-CDs-Tz might be due to shorter incubation time (1 h), which was used instead of 2h to mitigate the effect of radioactive decay.

The investigation of the internalization mechanism of the B-CDs-Cy3 was beyond the scope of this work. However, based on previously published works,[42, 43] it is reasonable to assume that internalisation occurs by a combination of the three mechanisms, i.e. clathrin- and caveolin-mediated endocytosis and micropinocytosis. The precise contribution of each individual pathway would require further investigation.

Cytotoxicity studies were carried out by incubation of the cells with increased concentrations of dots (0–160 µg/mL). The results showed >90 % cell survival after 48 and 72 h, indicating negligible cytotoxicity (Fig. 3d) and confirming the suitability of the nanosystems to move to *in vivo* experiments.

Radiolabelling, biodistribution and *in vivo* internalisation of mAb: To appropriately design the pre-targeting proof-of-concept experiments, the optimal time for the administration of the boron-rich component (this is, the time window in which the concentration of the mAb in the tumour is maximum) needed to be defined. PET is a minimally invasive, ultra-sensitive molecular imaging technique that enables the determination of the spatiotemporal distribution of a positron emitter-labelled molecule after administration in a living organism. Hence, it is ideally suited to investigate the accumulation of labelled entities in different organs and tissues in a time-resolved fashion. Here, this imaging technique was first used to investigate the biodistribution of [^{89}Zr]Zr-DFO-Trastuzumab in a breast cancer xenograft mouse model, generated by subcutaneous injection of HER2+ BT-474 cells in immunodeficient mice. BNCT has been traditionally applied to glioma, as this tumour does not metastasise out of the brain, thus facilitating localised neutron irradiation. This is not the case of breast cancer, which often metastasises through the whole body. The selection of a breast cancer model in the current study was for practical reasons; despite the clinical translation of our approach might be questionable in breast cancer, the model was appropriate for our proof of concept experiments.

Trastuzumab was radiolabelled with the long-lived radioisotope ^{89}Zr to assess long term distribution. Radiochemical yield of the purified [^{89}Zr]Zr-DFO-Trastuzumab was 78.7 ± 11.5 % (n = 3) with a radiochemical purity of >95 %, determined by iTLC, and an immune reactive fraction of 90 %, as determined by Lindmo assay.

Imaging experiments at different time points after intravenous administration showed the presence of radioactivity in the blood (represented by the activity measure in heart) even at 72 h and confirmed the long circulation time of the labelled mAb. Initial accumulation in the liver was also observed, followed by progressive clearance from this organ (Fig. 4a). High concentration of radioactivity could be observed in the tumour at t > 24h. Quantification of the images confirmed high

tumour uptake at 24 h, with statistically non-significant increase in accumulation at t = 48 h and a slight, statistically non-significant decrease at t = 72 h (Fig. 4b).

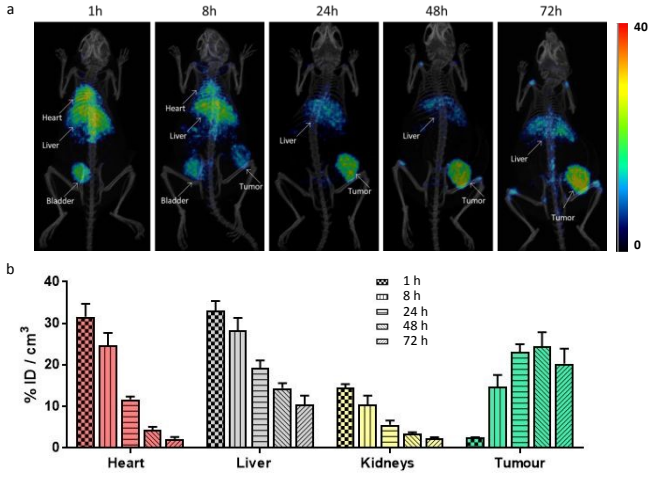

Figure 4. (a) Representative PET images (coronal projections) obtained at different times after administration of [^{89}Zr]Zr-DFO-Trastuzumab in BT-474 xenograft mice; images have been co-registered with computed tomography (CT) 3D-rendered images. Scale bar is in %ID/g; (b) accumulation of radioactivity in different organs at different times after administration of [^{89}Zr]Zr-DFO-Trastuzumab. Values correspond to average ± standard deviation, n=3.

In order to maximise the tumour uptake and prevent the occurrence of the click reaction in the blood, the most optimal time for B-CDs-tz injection, determined based on the maximum of the tumour-to-blood ratio of mAb, was determined to be t = 24–72 h. To further narrow down the time window for optimal pre-targeting protocol, longitudinal Trastuzumab cell internalization was taken into a closer examination. This is important, because only the mAb attached to the cell walls, but not the one internalized into the cell, can act as an effective partner for the click reaction with B-CDs-tz. To gain an insight into the eventual internalisation of Trastuzumab *in vivo*, we designed an experimental set-up based on labelling the mAb, either with ^{89}Zr- or ^{131}I. This method took advantage of a natural cellular process where iodine is cleaved off and released from the cell, whereas zirconium remains in the cell after internalisation. Hence, by determining the uptake ratio between [^{131}I]I-mAb and [^{89}Zr]Zr-mAb, mAb internalisation over time could be estimated. Experimentally, ^{89}Zr- and ^{131}I-labelled trastuzumab were mixed in a 1:1 ratio, and tumour bearing mice (n = 4) were injected intravenously (100 µg per animal). In both cases, the labelling process did not affect immunoreactivity, as determined by Lindmo assay[34] (90 % and 97 % for ^{89}Zr- and ^{131}I-labelled mAb, respectively). At t = 24 and 48 h after administration, the animals were sacrificed (n = 2 per time point), the tumours were harvested and the amount of radioactivity in the tumour for each radionuclide was determined using gamma spectrometry. Results showed estimated internalisation ratios of 55 % and 65 % at t = 24 and 48 h, respectively (^{89}Zr-24h: 11.2 ± 0.2 %ID/g, ^{89}Zr-48h: 13.7 ± 1.8 %ID/g, ^{131}I-24h: 5.0 ± 1.0 %ID/g, ^{131}I-48h: 4.8 ± 0.5 %ID/g) thus confirming that approximately half of the mAb remained in the cell membrane amenable for the click reaction at t = 24 h. The use of mAbs with less internalisation capacity *in vivo* might further improve the tumour uptake of the B-CDs-tz and allow for administration of the CDs at later times (e.g. 48–72h), preventing the click reaction to occur in blood and increase bioavailability of B-CDs-tz. Hence, the observed partial internalisation can be regarded as room for improvement in future experiments.

Nevertheless, for the purpose of this pilot study, and based on the internalization experiments and optimal tumour-to-blood ratio of Trastruzumab, it was concluded that injection of B-CDs-tz 24 h after the introduction of mAb-TCO would result in the most effective treatment protocol.

Proof of concept in *in vivo* studies

The main objective of the current work was to determine whether pre-targeting strategy results in increased boron uptake in the tumour. Over the years, different techniques to quantify the amount of boron in the tumour have been developed,[44] but most of them are based on therapeutically less relevant *ex vivo* approaches. Here, we envisaged the use of PET imaging with positron emitter radiolabelled boron carrier (B-CDs) to determine the pre-targeting efficacy. The concentration of radioactivity in the tumour was used as a surrogate of the boron concentration in this tissue. Considering the (expected) fast pharmacokinetics of B-CDs-tz, fluorine-18 (^{18}F; $t_{1/2}$ = 109.77 min) was selected as radiolabel due to the excellent emission properties (almost 100% positron emission, low positron energy) and high availability of this radionuclide. The radionuclide was introduced in the form of the pre-labelled prosthetic group [^{18}F]FPyTFP,[33] which has proven suitable for the radiolabelling of different biomolecules, e.g. peptides.[45] This prosthetic group could be obtained in 14 % non-decay corrected yield (total preparation time ca. 60 minutes) and >99% radiochemical purity as determined by HPLC. Taking advantage of the presence of free amino groups on the surface of the dots, almost quantitative labelling could be achieved by incubation (10 min, 70 °C, PBS) with [^{18}F]FPyTFP, as confirmed by radio-TLC (Fig. 3b).

Visual inspection of the images at the whole body level (Fig. 5a) showed fast accumulation of radioactivity in the kidneys and progressive elimination *via* urine both for the control and the study groups, suggesting that [^{18}F]B-CDs-tz is below the glomerular filtration limit of the kidneys. No apparent accumulation was observed in any other organ, except in the liver at short times after administration.

To quantify this data, volumes of interest were drawn in different organs. Similar time-activity profiles were obtained for both the study and control groups (Figs. 5c and 5d). The time activity curves in the heart, which can be considered as a surrogate of time-activity curves in blood, showed fast clearance in both groups, confirming our initial hypothesis that small CDs circulate in the blood for a short period of time. The accumulation of radioactivity in lungs, liver and kidneys showed a similar profile, with no significant differences between the groups. Most importantly, accumulation in the

View Article Online
DOI: 10.1039/D0TB01880E

tumour showed different profiles for both groups (Fig. 5e). While clearance profile in the control group followed the trend observed for other organs, higher retention could be observed in the tumours of the study group, with values remaining stable over the whole duration of the imaging session. Additionally, values obtained at 25–45 min post administration of [^{18}F]B-CDs-tz were significantly higher for the study group, providing with a proof that the click reaction occurs in the tumour. These differences can be easily observed even by visual inspection of axial-view representation of slices of the PET images at 25–45 min after administration that clearly show increased [^{18}F]B-CDs-tz accumulation in the tumour of the study, but not the control group (Fig. 5b).

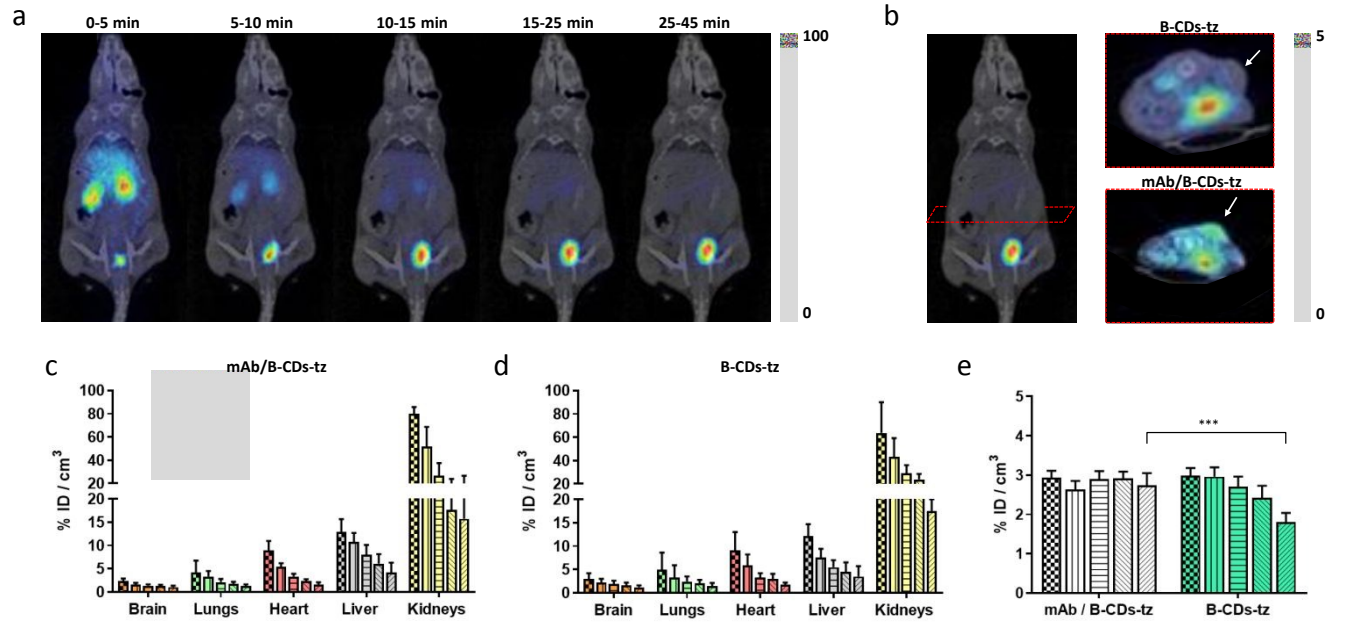

Figure 5. (a) Representative PET images (coronal projections) obtained at different times after administration of [^{18}F]B-CDs-tz; images have been co-registered with representative computed tomography (CT) slices. Scale bar is in %ID/g; (b) representative axial slices in the region of the tumour corresponding to PET-CT images obtained after administration of [^{18}F]B-CDs-tz (time frame 25–45 min) for control (B-CDs-tz) and study (mAb/B-CDs-tz) groups. Scale bar is in %ID/g; (c, d) accumulation of radioactivity in different organs at different times after administration of [^{18}F]B-CDs-tz, obtained for the study (mAb/B-CDs-tz) (c) and control (B-CDs-tz) (d) groups; (e) accumulation of radioactivity in the tumour at different times after administration of [^{18}F]B-CDs-tz for the study and control groups; significant differences are found in the time frame 25–45 min (P = 0.0005).

Conclusions

In conclusion, we show that the use of a pre-targeting strategy enhances the accumulation of boron-rich carbon dots in the tumour. Due to potential increase in selectivity of boron delivery at the tumour this approach represents a valuable strategy for application in BNCT. Furthermore, this methodology has the potential to be used in other pre-targeting-based therapeutic approaches in which a fast clearance of the second component is paramount to decrease off-target side effects, e.g. in radionuclide therapy. It allows for easy modifications, supports the use of a variety of antibodies, and allows for alternative administration routes (e.g. continuous slow infusion) that may contribute to enhance tumour accumulation. Allowing protocol modifications, the methodology presented in this work creates a base for the development of new therapeutic strategies that may improve the efficacy of current therapeutic approaches available on the market.

Conflicts of interest

There are no conflicts to declare.

Acknowledgements

Financial support for this work was provided by the European Commission under the H2020-MSCA-ITN-2015 program (grant agreement Nº. 675417) and the Spanish Ministry of Economy and Competitiveness (CTQ2017-87637-R). The work was performed under the Maria de Maeztu Units of Excellence Program (Grant No. MDM-2017-0720).

Notes and references

1 1. *Global Cancer Facts & Figures 4th Edition*, American Cancer Society, Atlanta, 2018.

2 2. G. L. Locher, *American Journal of Roentgenology Radium Therapy and Nuclear Medicine*, 1936, **36**, 1-13.

3 3. R. F. Barth, J. A. Coderre, M. G. H. Vicente and T. E. Blue, *Clin. Cancer Res.*, 2005, **11**, 3987-4002.

4 4. J. P. Pouget and S. J. Mather, *Eur. J. Nucl. Med.*, 2001, **28**, 541-561.

5 5. K. Hu, Z. Yang, L. Zhang, L. Xie, L. Wang, H. Xu, L. Josephson, S. H. Liang and M. R. Zhang, *Coord. Chem. Rev.*, 2020, **405**, 213139.

6 6. R. F. Barth, P. Mi and W. Yang, *Cancer Commun.*, 2018, **38**, 1-15.

7 7. G. N. Laurenţia and A. M. Rodica, *Therapeutics, Pharmacology and Clinical Toxicology*, 2015, **19**, 135-140.

8 8. R. F. Barth and J. C. Grecula, *Appl. Radiat. Isot.*, 2020, **160**, 109029.

9 9. E. Zavjalov, A. Zaboronok, V. Kanygin, A. Kasatova, A. Kichigin, R. Mukhamadiyarov, I. Razumov, T. Sycheva, B. J. Mathis, S. E. B. Maezono, A. Matsumura and S. Taskaev, *Int. J. Radiat Biol.*, 2020, DOI: 10.1080/09553002.2020.1761039.

10 10. M. Suzuki, *International Journal of Clinical Oncology*, 2020, **25**, 43-50.

11 11. Z. Yinghuai and N. S. Hosmane, *Future Med Chem*, 2013, **5**, 705-714.

12 12. Z. Yinghuai and S. H. Narayan, *Pure Appl. Chem.*, 2018, **90**, 653-663.

13 13. T. O. B. Olusanya, G. Calabrese, D. G. Fatouros, J. Tsibouklis and J. R. Smith, *Biophys. Chem.*, 2019, **247**, 25-33.

14 14. M. J. Luderer, B. Muz, K. Alhallak, J. Sun, K. Wasden, N. Guenthner, P. de la Puente, C. Federico and A. K. Azab, *Pharm. Res.*, 2019, **36**, 144.

15 15. W. Lee, S. Sarkar, H. Ahn, J. Y. Kim, Y. J. Lee, Y. Chang and J. Yoo, *Biochem. Biophys. Res. Commun.*, 2020, **522**, 669-675.

16 16. R. Tietze, H. Unterweger, S. Dürr, S. Lyer, L. Canella, P. Kudejova, F. M. Wagner, W. Petry, N. Taccardi and C. Alexiou, *Appl. Radiat. Isot.*, 2015, **106**, 151-155.

17 17. E. Oleshkevich, A. Morancho, A. Saha, K. M. O. Galenkamp, A. Grayston, S. G. Crich, D. Alberti, N. Protti, J. X. Comella, F. Teixidor, A. Rosell and C. Viñas, *Nanomedicine: Nanotechnology, Biology, and Medicine*, 2019, **20**, 101986.

18 18. K. Dukenbayev, I. V. Korolkov, D. I. Tishkevich, A. L. Kozlovskiy, S. V. Trukhanov, Y. G. Gorin, E. E. Shumskaya, E. Y. Kaniukov, D. A. Vinnik, M. V. Zdorovets, M. Anisovich, A. V. Trukhanov, D. Tosi and C. Molardi, *Nanomaterials*, 2019, **9**, 494.

19 19. M. Yamagami, T. Tajima, K. Ishimoto, H. Miyake, H. Michiue and Y. Takaguchi, *Heteroat. Chem*, 2018, DOI: 10.1002/hc.21467.

20 20. Z. Yinghuai, A. T. Peng, K. Carpenter, J. A. Maguire, N. S. Hosmane and M. Takagaki, *J. Am. Chem. Soc.*, 2005, **127**, 9875-9880.

21 21. T. H. Ferreira, M. C. Miranda, Z. Rocha, A. S. Leal, D. A. Gomes and E. M. B. Sousa, *Nanomaterials*, 2017, **7**, 82.

22 22. G. Ciofani, V. Raffa, A. Menciassi and A. Cuschieri, *Nanoscale Research Letters*, 2009, **4**, 113-121.

23 23. C. Y. Wu, J. J. Lin, W. Y. Chang, C. Y. Hsieh, C. C. Wu, H. S. Chen, H. J. Hsu, A. S. Yang, M. H. Hsu and W. Y. Kuo, *Colloids Surf. B. Biointerfaces*, 2019, **183**, 110387.

24 24. J. Wang, L. Chen, J. Ye, Z. Li, H. Jiang, H. Yan, M. Y. Stogniy, I. B. Sivaev, V. I. Bregadze and X. Wang, *Biomacromolecules*, 2017, **18**, 1466-1472.

25 25. K. R. Pulagam, K. B. Gona, V. Gómez-Vallejo, J. Meijer, C. Zilberfain, I. Estrela-Lopis, Z. Baz, U. Cossío and J. Llop, *Molecules*, 2019, **24**, 3609.

26 26. A. Rondon and F. Degoul, *Bioconjugate Chem.*, 2020, **31**, 159-173.

27 27. O. Keinänen, J. M. Brennan, R. Membreno, K. Fung, K. Gangangari, E. J. Dayts, C. J. Williams and B. M. Zeglis, *Mol. Pharm.*, 2019, **16**, 4416-4421.

28 28. R. Membreno, B. E. Cook and B. M. Zeglis, *Journal of Visualized Experiments*, 2019, DOI: 10.3791/59041.

29 29. F. C. Watering, M. Rijpkema, M. Robillard, W. J. Oyen and O. C. Boerman, *Frontiers in Medicine*, 2014, DOI: 10.3389/fmed.2014.00044.

30 30. B. M. Zeglis, K. K. Sevak, T. Reiner, P. Mohindra, S. D. Carlin, P. Zanzonico, R. Weissleder and J. S. Lewis, *J. Nucl. Med.*, 2013, **54**, 1389-1396.

31 31. J. Pellico, I. Fernández-Barahona, M. Benito, Á. Gaitán-Simón, L. Gutiérrez, J. Ruiz-Cabello and F. Herranz, *Nanomedicine: Nanotechnology, Biology, and Medicine*, 2019, **17**, 26-35.

32 32. J. P. Holland, Y. Sheh and J. S. Lewis, *Nucl. Med. Biol.*, 2009, **36**, 729-739.

33 33. D. E. Olberg, J. M. Arukwe, D. Grace, O. K. Hjelstuen, M. Solbakken, G. M. Kindberg and A. Cuthbertson, *J. Med. Chem.*, 2010, **53**, 1732-1740.

34 34. T. Lindmo, E. Boven, F. Cuttitta, J. Fedorko and P. A. Bunn Jr, *J. Immunol. Methods*, 1984, **72**, 77-89.

35 35. X. Xu, R. Ray, Y. Gu, H. J. Ploehn, L. Gearheart, K. Raker and W. A. Scrivens, *J. Am. Chem. Soc.*, 2004, **126**, 12736-12737.

36 36. W. Su, H. Wu, H. Xu, Y. Zhang, Y. Li, X. Li and L. Fan, *Materials Chemistry Frontiers*, 2020, **4**, 821-836.

37 37. K. Siwawannapong, R. Zhang, H. Lei, Q. Jin, W. Tang, Z. Dong, R. Y. Lai, Z. Liu, A. Kamkaew and L. Cheng, *Theranostics*, 2020, **10**, 62-73.

38 38. S. Wan, Y. Yu, J. Pu and Z. Lu, *RSC Advances*, 2015, **5**, 19236-19240.

39 39. Q. Ye, F. Yan, D. Shi, T. Zheng, Y. Wang, X. Zhou and L. Chen, *J. Photochem. Photobiol. B: Biol.*, 2016, **162**, 1-13.

40 40. F. Yan, Y. Jiang, X. Sun, Z. Bai, Y. Zhang and X. Zhou, *Microchimica Acta*, 2018, **185**, 424.

41 41. D. Berek, *J. Sep. Sci.*, 2010, **33**, 315-335.

42 42. S. Zhu, L. Wang, N. Zhou, X. Zhao, Y. Song, S. Maharjan, J. Zhang, L. Lu, H. Wang and B. Yang, *Chem. Commun.*, 2014, **50**, 13845-13848.

43 43. Y. Wei, X. Jin, T. Kong, W. Zhang and B. Zhu, *Cell Prolif.*, 2019, **52**, e12586.

44 44. A. Wittig, J. Michel, R. L. Moss, F. Stecher-Rasmussen, H. F. Arlinghaus, P. Bendel, P. L. Mauri, S. Altieri, R. Hilger, P. A. Salvadori, L. Menichetti, R. Zamenhof and W. A. G. Sauerwein, *Crit. Rev. Oncol. Hematol.*, 2008, **68**, 66-90.

View Article Online
DOI: 10.1039/D0TB01880E

45 45. W. G. Lesniak, R. C. Mease, S. Chatterjee, D. Kumar, A. Lisok, B. Wharram, V. R. Kalagadda, L. A. Emens, M. G. Pomper and S. Nimmagadda, *Molecular Imaging*, 2019, DOI: 10.1177/1536012119852189.

46

View Article Online
DOI: 10.1039/D0TB01880E

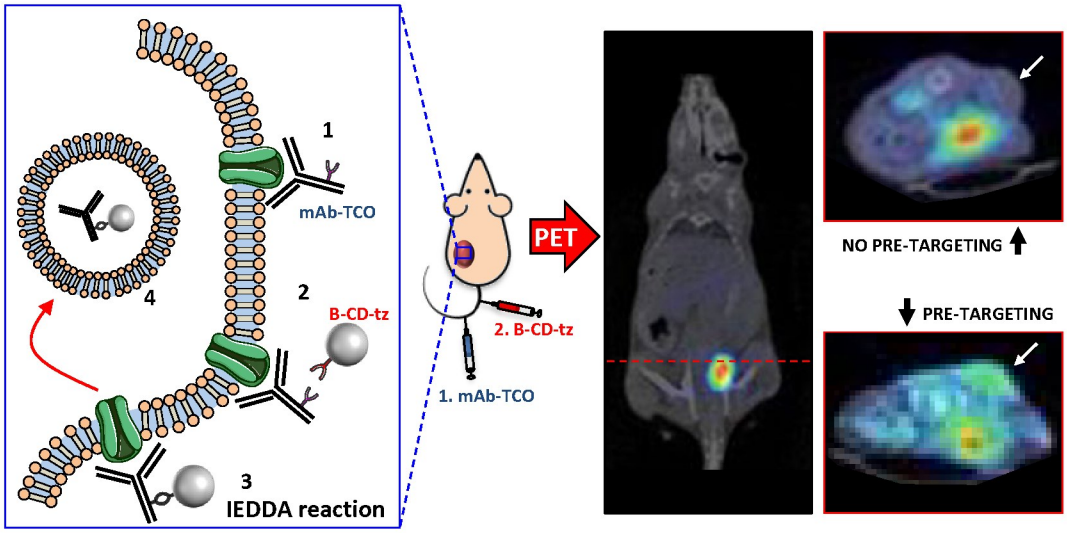

Tetrazine-functionalised boron-rich carbon dots show fast clearance and enhanced tumour accumulation under pre-targeting conditions as demonstrated using positron emission tomography.